Deep Contextual Recurrent Residual Networks for Scene Labeling

T. Hoang Ngan Le [1]   **Chi Nhan Duong** [1,2]   **Ligong Han** [1]   **Khoa Luu** [1]   **Marios Savvides** [1]   **Dipan Pal** [1]

Abstract

Designed as extremely deep architectures, deep residual networks which provide a rich visual representation and offer robust convergence behaviors have recently achieved exceptional performance in numerous computer vision problems. Being directly applied to a scene labeling problem, however, they were limited to capture long-range contextual dependence, which is a critical aspect. To address this issue, we propose a novel approach, **Contextual Recurrent Residual Networks (CRRN)** which is able to simultaneously handle rich visual representation learning and long-range context modeling within a fully end-to-end deep network. Furthermore, our proposed end-to-end CRRN is completely trained from scratch, without using any pre-trained models in contrast to most existing methods usually fine-tuned from the state-of-the-art pre-trained models, e.g. VGG-16, ResNet, etc. The experiments are conducted on four challenging scene labeling datasets, i.e. Sift-Flow, CamVid, Stanford background and SUN datasets, and compared against various state-of-the-art scene labeling methods.

1. Introduction

Scene labeling has played an important role in many applications in computer vision and machine learning. This problem is known as semantic segmentation and refers to associating one class to each pixel in a scene image. To address this issue, a large body of researches have recently proposed different approaches mainly focusing on contextual information via recurrent neural network (Shuai et al., 2015; Fan et al., 2016; Yang et al., 2014; Shotton et al., 2006) or enriching visual representations via convolutional

[1]CyLab Biometrics Center and the Department of Electrical and Computer Engineering,Carnegie Mellon University, Pittsburgh, PA, USA.
[2]Computer Science and Software Engineering, Concordia University, Montreal, Quebec, Canada.
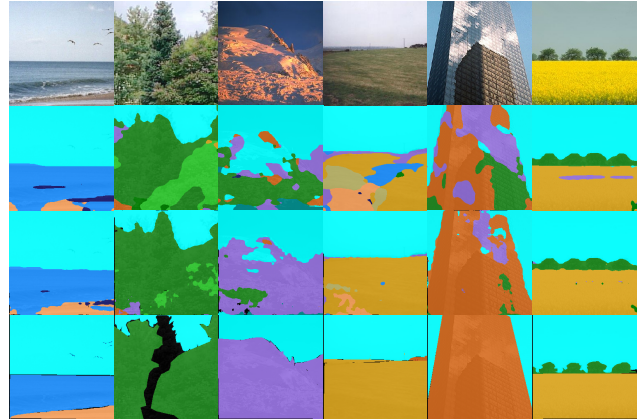.   Correspondence to: T. Hoang Ngan Le <thihoanl@andrew.cmu.edu>.

Figure 1. Examples of scene labeling results. From top to bottom: the input images, the segmentation results from (Shuai et al., 2016), our CRRN segmentation results, and the ground truth.

neural network (Farabet et al., 2013; Long et al., 2015; Pinheiro & Collobert, 2014; Zheng et al., 2015). However, scene labeling problem in the real world needs both information of the context dependencies and visual representation. For example, powerful visual representation is capable to discriminate a road from a beach; but it may not effective enough to tell a patch of sand belongs to the side of a road or to a beach. In such circumstance, the context presented in the whole scene can show its advantage to describe them. Indeed, the roles of contextual information and powerful descriptive visual representation are equally important in the scene labeling problem.

To effectively address the scene labeling problem, we propose a novel deep network named **Contextual Recurrent Residual Network (CRRN)** that inherits all the merits of sequence learning information and residual learning in order to simultaneously model *long-range contextual information* and learn *powerful visual representation* within a *single deep network*. Our proposed CRRN deep network consists of three parts corresponding to sequential input data, sequential output data and hidden state. Each unit in hidden state is designed as a combination of two components: a context-based component via sequence learning and a visual-based component via residual learning. That means, each hidden unit in our proposed CRRN simultaneously (1) learns long-range contextual dependencies via

context-based component. The relationship between the current unit and the previous units is performed as sequential information under an undirected cyclic graph (UCG) and (2) provides powerful encoded visual representation via residual component which contains blocks of convolution and/or batch normalization layers equipped with an identity skip connection. Furthermore, unlike previous scene labeling approaches (Shuai et al., 2015; Fan et al., 2016; Byeon et al., 2015), our method is not only able to exploit the long-range context and visual representation but also formed under a fully-end-to-end trainable system that effectively leads to the optimal model. In contrast to other existing deep learning network which are based on pre-trained models, our fully-end-to-end CRRN is completely trained from scratch.

2. Related Work

Scene labeling is arguably one of the hardest challenges in computer vision. It requires the algorithms to have much more finesse than those that are only required to tackle image scale object recognition for instance. Nonetheless, a lot of studies have focused on this challenging problem in the past and have made considerable progress recently. Generally, scene labeling methods can be divided into three categories as follows.

Graphical model approaches: In the past, using traditional vision techniques, scene labeling was approached from a undirected graphical model paradigm utilizing markov random fields (MRF) and conditional random fields (CRF) (Liu et al., 2016; Tighe & Lazebnik, 2010; Yang et al., 2014). In (Liu et al., 2016), SIFT flow was utilized as features, whereas as (Tighe & Lazebnik, 2010) utilized k-nearest neighbors in a retrieval dataset to classify superpixels. One of the first studies to utilize contextual information within the MRF framework was (Yang et al., 2014). Similar efforts have been made for using CRFs on unary and pairwise image features (Shotton et al., 2006). Parametric and non-parametric techniques were also combined to model global order dependencies to provide more information and context (Shuai et al., 2015). Higher order dependencies were also modeled using a fully connected graph (Zhang & Chen, 2012; Roy & Todorovic, 2014).

ConvNet-based approaches: In recent years, deep learning techniques have started to become ubiquitous in scene labeling. One of the first studies to apply convolutional neural networks (deep CNNs) to scene labeling was (Farabet et al., 2013), which stacked encompassing windows from different scales to serve as context. This inspired other studies in which fully convolutional networks were used instead (Long et al., 2015) utilizing higher model complexity. Both these techniques used filter based models to incorporate context. Recently, recurrent models have

started to gain popularity. For example (Pinheiro & Collobert, 2014), where the image is passed through a CNN multiple times in sequence *i.e.* the output of the CNN is fed into the same CNN again. As an interesting study, (Zheng et al., 2015) modeled a CRF as a neural network that is applied iteratively to an input, thereby qualifying as a recurrent model. Inference is done through convergence of the neural network output to a fixed point. Recently, deep residual networks (ResNets) (He et al., 2016a) have emerged as a family of extremely deep architectures showing compelling accuracy and desirable convergence behaviors. They consist of blocks of convolutional and/or batch normalization layers equipped with an identity skip connection. The identity connection helps to address the vanishing gradient problem and allows the ResNets to robustly train using standard stochastic gradient descent despite very high model complexity. This enables ResNets to extract very rich representations of images that perform exceedingly well in image recognition and object detection challenges (He et al., 2016b). The extremely deep architectures in ResNets show compelling accuracy and robust convergence behaviors and achieve state-of-the-art performance on many challenging computer vision tasks on ImageNet (Russakovsky et al., 2014), PASCAL Visual Object Classes (VOC) Challenge (Everingham et al., 2015) and Microsoft Common Objects in Context (MS COCO) (Lin et al., 2014) competitions. Nonetheless, they are feed forward models that do not explicitly encode contextual information and typically cannot be applied to sequence modeling problems. On the other hand, they are able to *effectively learn visual representations but limited to model long-range context explicitly*

Recurrent-based approaches: In recent years, vision data is being interpreted as sequences leading to the successful application of RNNs (and their variants, e.g. Long-Short Term Memories (LSTMs), Gated Recurrent Units (GRUs), etc.,) to vision problems. For instance, (Zuo et al., 2015) and (Graves, 2012) applied 1-D RNNs and multi-dimensional RNNs to model contextual dependencies in object recognition/image classification and offline handwriting recognition respectively. 2-D LSTMs instead were applied to scene parsing (Byeon et al., 2015), Lately, scene labeling (Shuai et al., 2015), object segmentation (Visin et al., 2015), have been reformulated as sequence learning, thereby allowing RNNs to be applied directly. Scene labeling, in particular, has seen the use of RNNs coupled with Directed Acyclic Graphs (DAGs) to model an image as a sequence (Shuai et al., 2015; Fan et al., 2016; Byeon et al., 2015). There have also been a few studies that utilize RNNs to compute visual representations (Mnih et al., 2014; Donahue et al., 2015). Clearly, RNN-based approaches are *effective in context modeling but lack the ability to learn visual representation.*
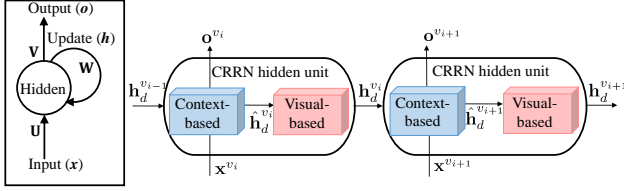
Figure 2. The proposed CRRN and the unfolding in time of the computation involved in its forward procedure.

Figure 3. Decomposition of UCG into four DAGs. From left to right: southeast, southwest, northwest and northeast, where ● denotes as a vertex

Figure 4. The forward procedure of CRRN at vertex $\mathbf{v}_i$ of one CRRN unit with two components corresponding to context information modeling and visual representation learning

Drawbacks of the current approaches are: (1) The ConvNet-based approaches model makes use of convolutional filters which allow them to learn the short-range context of surrounding neighbors designed by these filers. Therefore they are limited to generalize to long-range contexts dependencies. (2) The RNN-based approaches usually utilize a feature extractor that is independent of the sequence modeling framework, in many cases being trained component wise and not end-to-end (Shuai et al., 2016). (3) Purely RNN based approaches fail to extract robust visual features during sequence learning itself. This is due to simple linear models being used as the recurrent internal models.

3. Proposed Contextual Recurrent Residual Networks (CRRN)

This section presents our proposed Contextual Recurrent Residual Networks (CRRN) for scene labeling problem. The proposed CRRN architecture is first described in Sec.3.1. Then, the model learning and the inference are detailed in Sec. 3.2 and Sec. 3.3, respectively.

3.1. The Proposed Network Architecture

Our proposed CRRN is designed as a composition of multiple CRRN units. Each of them consists of input, hidden, and output units. In the core of each CRRN hidden unit, two components, i.e. context-based and visual-based components, are employed to simultaneously handle two significant tasks. The former helps to handle the contextual knowledge embedding process while the latter tries to increase the robustness of visual representation extracted by the model. With this structure, one component can benefit from the other and provide more robust output as a result. On one hand, the powerful visual representation from the visual-based component allows the model to have better descriptors for each local patch and results in the better contextual knowledge embeddings. On the other hand, with better memory contextual dependencies from context-based component, highly discriminative descriptors can be extracted. Fig. 2 demonstrates the folding CRRN on the left and unfolding CRRN in time on the right.
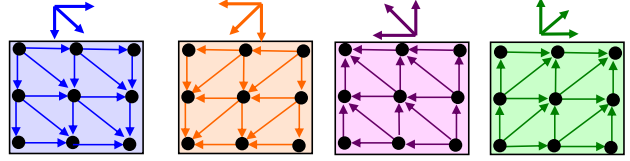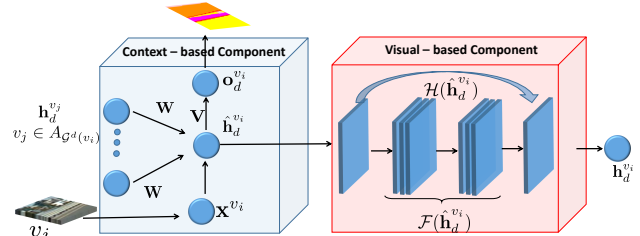
Moreover, unlike previous approaches that are only able to capture the short-range context presented in small local input patches, our CRRN aims at modeling larger-range context by utilizing a graph structure over an image. As a result, the long-range contextual dependencies among different regions of an image can be efficiently modeled and, therefore, increasing the capability of the entire model. In particular, given an input image, it is first divided into N non-overlapping blocks and their interactions are represented as an undirected cyclic graph (UCG). However, an UCG is unable to unroll as the forward-backward style deep model (Shuai et al., 2016; Fan et al., 2016) due to its loopy structures. Therefore, to address this issue, we first decompose the UCG into four directed acyclic graphs (DAGs) along southeast, southwest, northwest and northeast directions as given in Fig. 3. Then the contextual dependencies presented in each DAG are modeled by our CRRN. Finally, these information is combined to produce the final prediction.

Formally, an input image $\mathbf{I}$ is first divided into N non-overlapping blocks $\{v_i\}_{i=1,2,..,N}$. Each block is then considered as a vertex in four DAGs $\mathcal{G}^1$, $\mathcal{G}^2$, $\mathcal{G}^3$, $\mathcal{G}^4$ corresponding to the four directions. Each DAG is formed as $\mathcal{G}^d = \{\mathcal{V}, \mathcal{E}\}|_{d=1}^4$, where $\mathcal{V} = \{v_i\}_{i=1,2,..,N}$, and $\mathcal{E} = \{e_{ij}\}$ is the edge set where each edge e_{ij} represents the relationship between vertices v_i and v_j. For each direction $\mathcal{G}^d$, let $\mathcal{A}_{\mathcal{G}^d(v_i)}$ and $\mathcal{S}_{\mathcal{G}^d(v_i)}$ be the predecessor and successor sets of v_i. Depending on the relationships between vertices in $\mathcal{G}^d$, all vertices are organized into a sequence and fed into the CRRN structure for modeling. As illustrated in Fig. 4, the i-th CRRN unit takes an input of $\mathbf{x}^{v_i}$ and the hid-
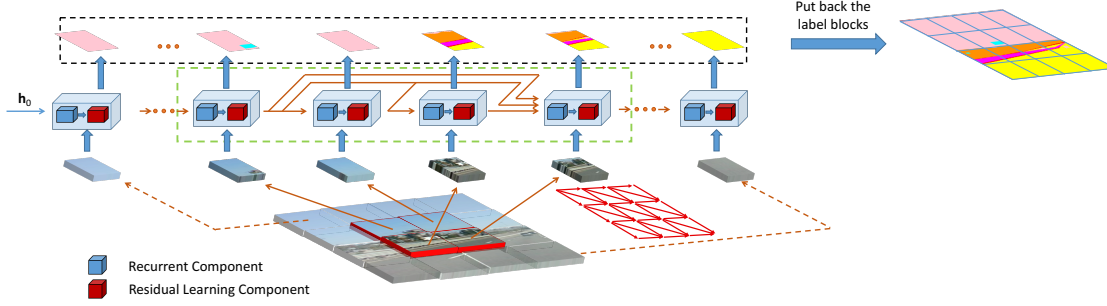
Figure 5. An illustration of our proposed CRRN architecture at one direction (southeast)

den state of all vertices in the predecessor set $\mathcal{A}_{\mathcal{G}^d(v_i)}$. The input $\mathbf{x}^{v_i}$ can be computed as $\mathbf{x}^{v_i} = \text{vec}(v_i)$ where $\text{vec}(\cdot)$ is the vectorization operator. The following will detail the proposed CRRN architecture with two main tasks: (1) the contextual information embedding via sequence learning, and (2) the visual representation learning.

3.1.1. CONTEXTUAL INFORMATION EMBEDDING

Starting with one DAG $\mathcal{G}^d$ at vertex v_i, the contextual relationship between the vertex v_i and its predecessor set $\mathcal{A}_{\mathcal{G}^d(v_i)}$ is expressed as a non-linear function over the current input x^{v_i} and the summation of hidden layers of all its predecessors in the context-based component as follows:

$$\hat{\mathbf{h}}_d^{v_i} = f_{\text{CONTEXT}}(\mathbf{x}^{v_i}, \mathcal{A}_{\mathcal{G}^d(v_i)}; \theta_1)$$
$$= \phi(\mathbf{U}\mathbf{x}^{v_i} + \sum_{v_j \in \mathcal{A}_{\mathcal{G}^d(v_i)}} \mathbf{W}\mathbf{h}_d^{v_j} + \mathbf{b}) \quad (1)$$

where $\mathbf{h}_d^{v_j}$ is the hidden state of vertex v_j belonging to predecessor set $\mathcal{A}_{\mathcal{G}^d(v_i)}$ of vertex v_i in the DAG $\mathcal{G}^d$, $\hat{\mathbf{h}}_d^{v_i}$ is the intermediate hidden state of vertex v_i and $\theta_1 = \{\mathbf{U}, \mathbf{W}, \mathbf{V}, \mathbf{b}\}$ is the parameters of context-based component representing the connection weights of input-to-hidden, predecessor-to-hidden and hidden-to-output; and the hidden bias, respectively. $\phi(\cdot)$ is the activation function, i.e. ReLU function.

3.1.2. VISUAL REPRESENTATION LEARNING

To further extract powerful visual representation as well as address the vanishing problem during modeling, we employ the visual-based component with residual learning technique. Given the intermediate hidden state $\hat{\mathbf{h}}_d^{v_i}$ of the vertex v_i provided by the context-based component, The representation $\mathbf{h}_d^{v_i}$ of each vertex v_i is computed as in Eqn. (2).

$$\mathbf{h}_d^{v_i} = f_{\text{VISUAL}}(\hat{\mathbf{h}}_d^{v_i}; \theta_2)$$
$$= \phi(\mathcal{F}(\hat{\mathbf{h}}_d^{v_i}) + \mathcal{H}(\hat{\mathbf{h}}_d^{v_i})) \quad (2)$$

where $\mathcal{F}$ denotes a residual function consisting of a two-layer convolutional network in residual-network style, i.e equipped with an residual learning connection as shown in Fig. 4. This network is a stack of two convolutional layers, i.e. alternating convolution, batch normalization and ReLU operations. Meanwhile, $\mathcal{H}$ is defined as an identity mapping, where $\mathcal{H}(\hat{\mathbf{h}}_d^{v_i}) = \hat{\mathbf{h}}_d^{v_i}$. θ_2 represents the parameters of the two-layer convolutional network.

The final output from the four DAGs are then combined using the following Eqn.3

$$\mathbf{o}^{v_i} = f(\mathbf{x}^{v_i}, \mathcal{A}_{\mathcal{G}(v_i)}; \theta_1, \theta_2)$$
$$= \sum_{d=1}^{4} \mathbf{V}\hat{\mathbf{h}}_d^{v_i} + \mathbf{b}_o \quad (3)$$

where $\mathbf{V}$ is the hidden-to-output weight matrix, $\mathbf{b}_o$ is output bias. The CRRN is then optimized to minimize the negative log-likelihood over the training data as follows.

$$\theta_1^*, \theta_2^* = \arg \min_{\theta_1, \theta_2} L(\theta_1, \theta_1) \quad (4)$$

$$L(\theta_1, \theta_1) = -\frac{1}{n} \sum_{v_i \in \mathcal{G}} \sum_j \log p(l_j^{v_i} | \mathbf{x}^{v_i}; \theta_1, \theta_2)$$
$$p(l_j^{v_i} | \mathbf{x}^{v_i}; \theta_1, \theta_2) = \frac{e^{f_{l_j^{v_i}}(\mathbf{x}^{v_i}, \mathcal{A}_{\mathcal{G}(v_i)}; \theta_1, \theta_2)}}{\sum_{c=1}^{C} e^{f_c(\mathbf{x}^{v_i}, \mathcal{A}_{\mathcal{G}(v_i)}; \theta_1, \theta_2)}} \quad (5)$$

where C is the number of classes; n is the number of images; $l_j^{v_i}$ is the correct label of j-th pixel in block v_i; and $f_{l_j^{v_i}}(\mathbf{x}^{v_i}, \mathcal{A}_{\mathcal{G}(v_i)}; \theta_1, \theta_2) = o_j^{v_i}$.

3.2. Model Learning

The optimal parameters can be obtained with the Stochastic Gradient Descent (SGD) algorithm given by

$$\theta_1 \leftarrow \theta_1 - \lambda \frac{\partial L}{\partial \theta_1}; \theta_2 \leftarrow \theta_2 - \lambda \frac{\partial L}{\partial \theta_2} \quad (6)$$

where λ denotes the learning rate. The derivatives are computed in the backward pass procedure is processed in the reverse order of forward propagation sequence as illustrated in Fig.6. Instead of looking at predecessor $\mathcal{A}_{\mathcal{G}^d(v_i)}$ in the forward pass, we are now taking a look at successor $\mathcal{S}_{\mathcal{G}^d(v_i)}$. It is clear that the backpropagation error at the intermediate hidden layer $d\hat{\mathbf{h}}_d^{v_i}$ comes from two sources: one from output $\frac{\partial \mathbf{o}_d^{v_i}}{\partial \hat{\mathbf{h}}_d^{v_i}}$ and the other one from hidden layer $\frac{\partial \mathbf{h}_d^{v_i}}{\partial \hat{\mathbf{h}}_d^{v_i}}$ whereas the backpropagation error at hidden layer $d\mathbf{h}_d^{v_i}$ comes from its successor set $\mathcal{S}_{\mathcal{G}^d(v_i)}$. i.e, $\sum_{v_k \in \mathcal{S}_{\mathcal{G}^d(v_i)}} \frac{\partial \mathbf{o}_d^{v_k}}{\partial \hat{\mathbf{h}}_d^{v_k}} \frac{\partial \hat{\mathbf{h}}_d^{v_k}}{\partial \mathbf{h}_d^{v_i}}$. To make it simple and general, we would like to express the parameters in a form without subscript $_d$. For example we will use $\mathbf{h}^{v_i}$ instead of $\mathbf{h}_d^{v_i}$. The derivative with respect to the model parameters $\{\mathbf{o}^{v_i}, \hat{\mathbf{h}}^{v_i}, \mathbf{h}^{v_i}, \mathbf{V}, \mathbf{U}, \mathbf{W}\}$ can be computed as follows.

$$d\mathbf{o}^{v_i} = \frac{\partial L}{\partial \mathbf{o}^{v_i}}$$

$$d\hat{\mathbf{h}}^{v_i} = \frac{\partial L}{\partial \mathbf{o}^{v_i}} \frac{\partial \mathbf{o}^{v_i}}{\partial \hat{\mathbf{h}}^{v_i}} + \left(\frac{\partial \mathbf{h}^{v_i}}{\partial \hat{\mathbf{h}}^{v_i}}\right)^T d\mathbf{h}^{v_i}$$

$$= \mathbf{V}^T d\mathbf{o}^{v_i} + \left(\frac{\partial \mathbf{h}^{v_i}}{\partial \hat{\mathbf{h}}^{v_i}}\right)^T d\mathbf{h}^{v_i}$$

$$d\mathbf{h}^{v_i} = \sum_{v_k \in \mathcal{S}_{\mathcal{G}^d(v_i)}} \mathbf{W}^T \frac{\partial L}{\partial \hat{\mathbf{h}}^{v_k}} \frac{\partial \hat{\mathbf{h}}^{v_k}}{\partial \mathbf{h}^{v_i}} \circ \phi'(\hat{\mathbf{h}}^{v_i})$$

$$= \sum_{v_k \in \mathcal{S}_{\mathcal{G}^d(v_i)}} \mathbf{W}^T d\hat{\mathbf{h}}^{v_k} \circ \phi'(\hat{\mathbf{h}}^{v_i}) \quad (7)$$

$$\nabla \mathbf{V} = \frac{\partial L}{\partial \mathbf{o}^{v_i}} \frac{\partial \mathbf{o}^{v_i}}{\partial \mathbf{V}} = d\mathbf{o}^{v_i} \left(\hat{\mathbf{h}}^{v_i}\right)^T$$

$$\nabla \mathbf{U} = \frac{\partial L}{\partial \mathbf{o}^{v_i}} \frac{\partial \mathbf{o}^{v_i}}{\partial \hat{\mathbf{h}}^{v_i}} \frac{\partial \hat{\mathbf{h}}^{v_i}}{\partial \mathbf{U}} = d\hat{\mathbf{h}}^{v_i} \circ \phi'(\hat{\mathbf{h}}^{v_i}) (\mathbf{x}^{v_i})^T$$

$$\nabla \mathbf{W} = \frac{\partial L}{\partial \mathbf{o}^{v_i}} \frac{\partial \mathbf{o}^{v_i}}{\partial \hat{\mathbf{h}}^{v_i}} \frac{\partial \hat{\mathbf{h}}^{v_i}}{\partial \mathbf{W}}$$

$$= \sum_{v_j \in \mathcal{S}_{\mathcal{G}}^d(v_i)} d\hat{\mathbf{h}}^{v_j} \circ \phi'(\hat{\mathbf{h}}^{v_j}) \left(\hat{\mathbf{h}}^{v_i}\right)^T$$

where $\circ$ represents the Hadamard product.

3.3. Inference

Given a testing image $\mathbf{I}$, we first divide $\mathbf{I}$ into N blocks v_i, $i = 1...N$. These blocks are then fed into four DAGs. The inference process of each pixel j in block v_i can be performed by finding the class label that maximizes the conditional probability given by

$$l_j^{v_i*} = \arg\max_c p(c|\mathbf{x}^{v_i}; \theta_1, \theta_2) \quad (8)$$

Finally, the prediction maps of all v_i are concatenated based on the location of block v_i in $\mathbf{I}$ for the final predic-
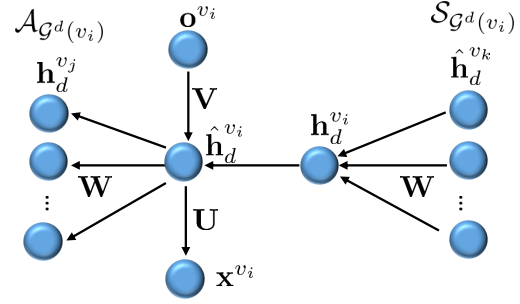

Figure 6. The backward procedure of CRRN at vertex $\mathbf{v}_i$

tion map. Fig. 5 illustrates the inference process of CRRN at one direction (southeast) as an example.

4. Experimental Results

In this section, we evaluate the efficiency of our proposed CRRN using four challenging and popular scene image labeling datasets, i.e. SiftFlow (Liu et al., 2009), CamVid (Brostow et al., 2008), Stanford Background (Gould et al., 2009) and SUN (Xiao et al., 2010).

4.1. Datasets and Measurements

SiftFlow Dataset (Liu et al., 2009) contains 2,688 images captured from 8 typical outdoor scenes, i.e. coast, forest, highway, inside city, mountain, open country, street, tall building. Each image is 256×256 and labeled with 33 semantic classes (ignore the background). To run the experiment, the dataset is separated into 2 subsets corresponding to 2,488 images for training and the rest for testing as in (Shuai et al., 2016).

CamVid Dataset (Brostow et al., 2008) is a road scene dataset which contains 701 high-resolution images of 4 driving videos captured at both day and dusk modes (Brostow et al., 2009). Each image is 960x720 and is labeled with 32 semantic classes. We follow the usual split protocol as given in (Tighe & Lazebnik, 2013) with 468 images for training and the rest for testing.

Stanford Background Dataset (Gould et al., 2009) contains 715 images annotated with 8 semantic classes. The dataset is randomly partitioned into 80% (572 images) for training and the rest (143 images) for testing with 5-fold cross validation.

SUN Dataset (Xiao et al., 2010) contains 16,873 images annotated with 3,819 semantic object categories. However, the numbers of images per category are highly unbalanced. Therefore, we choose the most common 33 categories for evaluation. The chosen dataset with these categories contains 6,433 images and is randomly partitioned into two subsets corresponding to 5,798 images for training and the

Figure 7. Comparison between our CRRN and (Shuai et al., 2016) in term of contextual dependencies learning. In each row, there are four images: input image (first column), the prediction labeling map of (Shuai et al., 2016) (second column), the contextual labeling map extracted from our CRRN (third column) and the ground truth labels. **(Best viewed in color.)**

rest for testing.

Measurements It has become common practice to report results using two metrics, namely, per-pixel accuracy (PA) and average per-class accuracy (CA). The first metric, i.e. $PA = \sum_i n_{ii} / \sum_i t_i$, is defined as the fraction of the number of pixels classified rightly over the number of pixels to be classified in total whereas the latter metric, i.e. $CA = (1/C) \sum_i (n_{ii}/t_i)$, is defined as the average of per-pixel accuracy of all the classes existing in the dataset. n_{ij} is the number of pixels of class i that were predicted to be class j, C is total number of classes and $t_i = \sum_j n_{ij}$ is the total number of pixels of class i.

4.2. Implementation Details

In this section, the implementation of our proposed model is discussed in details. The model is implemented in TensorFlow environment and runs in a machine of Core i7-6700 @3.4GHz CPU, 64.00 GB RAM and a single NVIDIA GTX Titan X GPU. In order to train the CRRN, each image in the training data is first divided into 64 (= 8×8) blocks. Next, these blocks are reorganized into four sequences based on their relationships in the four DAGs. Each block is vectorized and used as the input for the CRRN unit. Our CRRN architecture is then employed to simultaneously model the contextual dependencies between blocks in different directions as well as extract their compact and rich representation. The dimensionality of the hidden layer is set to 256 in the recurrent component and reshaped to 16×16 before going through the residual learn-

Table 1. Quantitative results and comparisons against *non-fine-tuned models* **2D-LSTM** (Byeon et al., 2015), **Recurrent CNN** (Pinheiro & Collobert, 2014), **Multi-scale Convnet** (Farabet et al., 2013), **Multi-CNN - rCPN** (Sharma et al., 2014), **Scene Graph Structure** (Souly & Shah, 2016), **CNN-65-DAG-RNN** (Shuai et al., 2016), **Sample&Filter + MRF** (Najafi et al., 2016), **Multi-scale RCNN** (Liang et al., 2015) on Siftflow dataset.

METHOD	PA	CA
2D-LSTM	70.1%	20.9%
Recurrent CNN	77.7%	29.8%
Multi-scale Convnet	78.5%	29.4%
Multi-CNN - rCPN	79.6%	33.6%
Scene Graph Structure	80.6%	45.8%
CNN-65-DAG-RNN	81.1%	48.1%
Sample&Filter + MRF	83.1%	44.3%
Multi-scale RCNN	83.5%	35.8%
Our CRRN	**84.7%**	**61.0%**

Table 2. Quantitative results and comparisons against *non-fine-tuned models* **Neural Decision Forest**s(Rota Bulo & Kontschieder, 2014), **SVM+MRF**(Tighe & Lazebnik, 2013) on CamVid dataset.

METHOD	PA	CA
Neural Decision Forests	82.1%	56.1%
SVM+MRF	83.9%	**62.5%**
Our CRRN	**84.4%**	54.8%

ing component. From our preliminary results, hidden layers with smaller number of hidden units are not powerful enough to capture both contextual information and visual representation in four DCGs. The optimal parameter values of the whole network are obtained via a stochastic gradient descent procedure with forward and backward passes. The learning rate is initialized to be 10^{-3}, and decays with the rate of 0.95 after 30 epochs. The whole model takes about 12.7 hours to train. For inference process, CRRN takes 0.058 second/image.

4.3. Scene Labeling Results

In order to make a fair comparison between our proposed CRRN and other state-of-the-art models, we divide the models into two groups: the ones trained using the benchmark datasets only; and the ones fine-tuned from other models which are trained over the large-scale datasets (i.e. ImageNet) or made used of deep network (i.e. VGG-verydeep-16) as their feature extractor. *Our CRRN falls into the first group where no pre-trained model is used.*

Comparing to the methods in the first group, the quantitative results of our approach with three benchmark datasets namely, Siftflow, Camvid, Stanford and SUN are reported
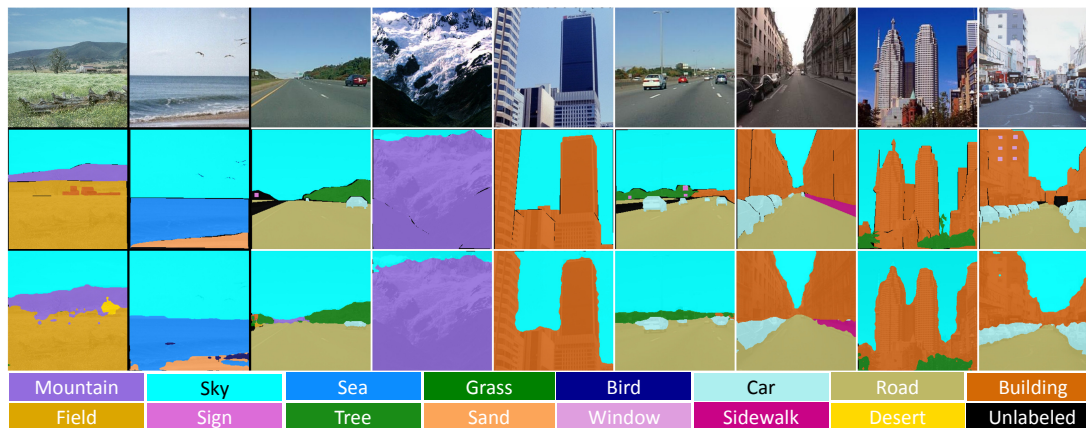
Figure 8. Examples of labeling results on SiftFlow dataset. Each column has three images: the input image (first row), its ground truth labels (second row) and our CRRN prediction labels (third row), respectively. **(Best viewed in color.)**

Table 3. Quantitative results and comparisons against *non-fine-tuned models* **2D-LSTM** (Byeon et al., 2015), **Recurrent CNN** (Pinheiro & Collobert, 2014), **Multi-scale Convnet** (Farabet et al., 2013), **Multi-scale RCNN** (Liang et al., 2015), **Scene Graph Structure** (Souly & Shah, 2016) on Stanford-background Dataset

METHOD	PA	CA
2D-LSTM	78.6%	68.8%
Recurrent CNN	80.2%	69.9%
Multi-scale Convnet	81.4%	76.0%
Multi-scale RCNN	83.1%	74.8%
Scene Graph Structure	84.6%	**77.3%**
Our CRRN	**85.23%**	75.2%

Table 4. Quantitative results and comparisons against *non-fine-tuned models* **CNN-65-DAG-RNN** (Shuai et al., 2016), **FCNN** (Long et al., 2015) on SUN dataset.

METHOD	PA	CA
CNN-65-DAG-RNN	71.51%	54.57%
FCNN	77.2%	**62.03%**
Our CRRN	**78.61%**	59.9%

Table 5. Quantitative results and comparisons against **CNN - Global Context** (Shuai et al., 2015), **FCNN** (Long et al., 2015), **VGG-conv5-DAG-RNN** (Shuai et al., 2016) with *fine-tuned models* on Siftflow dataset.

METHOD	PA	CA
CNN - Global Context	80.1%	39.7%
FCNN	85.2%	51.7%
VGG-conv5-DAG-RNN	**85.3%**	55.7%
Our CRRN	84.7%	**61.0%**

in Tables 1, 2, 3 and 4, respectively. The empirical results on three datasets show that our performance on both PA and CA scores are higher than state-of-the-art methods on larger dataset while giving quite competitive results on the smaller dataset. On larger Siftflow when we have big enough data for training, our proposed CRNN outperforms all other models in terms of both PA and CA scores. Our CA is 61.0% and PA is 84.0% compared to the next highest CA score of 48.1% (Shuai et al., 2016) and PA score of 83.5% (Liang et al., 2015) as shown in Tables 1. On the small dataset, take Camvid as an instance, when we just have about 468 images for training, our PA is still about 0.5% higher than the state-of-the-art method (Tighe & Lazebnik, 2013). On larger scale dataset such as SUN, our CRRN also achieves 1.41% higher than FCNN (Long et al., 2015) in term of PA score.

Figure 7 illustrates the advantages of our CRRN in term of modeling the contextual dependency presented in the image. Comparing to (Shuai et al., 2016), besides the local consistency between neighborhood regions, their semantic

coherence is better enhanced in our CRRN. For example, after training, our CRRN can capture the contextual knowledge such as the 'building' is not likely to appear in the 'sea' (i.e. the first case) or the 'desert' is not usually covered by the 'field' (i.e. the second case). As a result, while (Shuai et al., 2016) still has the problem of misclassification in its predictions, smoother and better labeling maps can be produced by our model. Our qualitative results on the datasets are further demonstrated in Figures 8, 9 and 10. As visualization, there exist many false positive cases where pixels are classified as unlabeled while they truly belongs to labeled classes. In such cases, our CRRN performs well to category the false positive pixels. Thank to the ability of simultaneously learning rich visual representation and modeling the context information, our model has
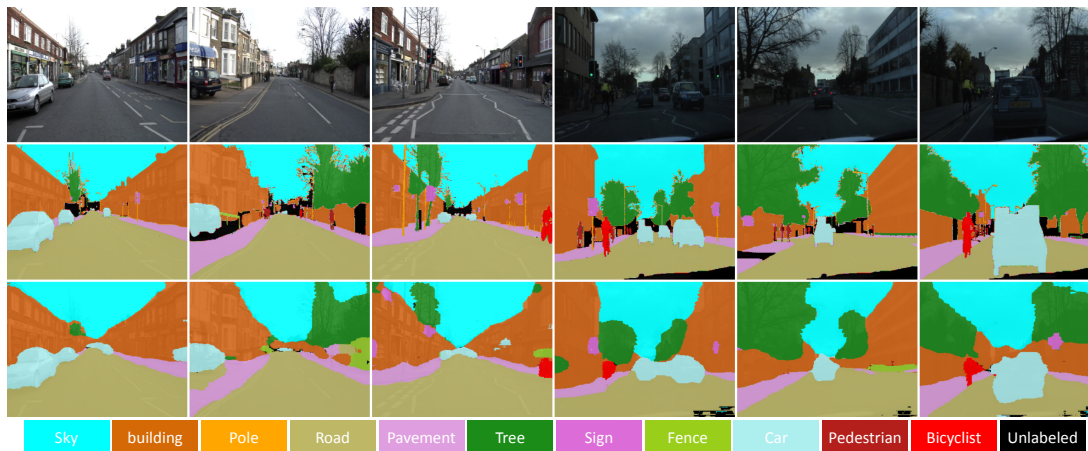
| Sky | building | Pole | Road | Pavement | Tree | Sign | Fence | Car | Pedestrian | Bicyclist | Unlabeled |

Figure 9. Examples of labeling results on CamVid dataset. Each column has three images: the input image (first row), its ground truth labels (second row) and our CRRN prediction labels (third row), respectively. **(Best viewed in color.)**

| Bridge | Building | Bus | Car | Crosswalk | Field | Grass | Mountain | Person |
| Road | Sand | Sea | Sidewalk | Tree | Sky | Window | Staircase | Unlabeled |

Figure 10. Examples of labeling results on SUN dataset. Each column has three images: the input image (first row), its ground truth labels (second row) and our CRRN prediction labels (third row), respectively. **(Best viewed in color.)**

better memory of contextual dependency and gives higher discriminative descriptors for each local patch

Furthermore, we also compare our CRRN with other fine-tuned methods on SiftFlow as shown in Table 5. In this group, most existing fine-tune methods (Shuai et al., 2015; Long et al., 2015; Shuai et al., 2016) are trained on large-scale data and make use of powerful feature extractor while our CRRN is a non fine-tune model and trained on Siftflow only. From these results, one can see that our CRRN model archives the best CA score (61.0%) compared to the state-of-the-art (55.7%) (Shuai et al., 2016) while giving a competitive PA score. We believe that given enough data, our CRRN performance can be boosted and is competitive to these models. We leave this as future work.

5. Conclusion

This paper presents a novel Contextual Recurrent Residual Networks (CRRN) approach, which is able to simultaneously model the long-range context dependencies and learn rich visual representation. The proposed CRRN is designed as a fully end-to-end deep learning framework and is able to make use the advantages of both sequence modeling and residual learning techniques. Our CRRN network contains three parts corresponding to sequential input data, sequential output data and hidden CRRN unit. Each hidden CRRN unit has two main components: context-based component to model the context dependencies and visual-based component to learn the visual representation. Our proposed end-to-end CRRN is completely trained from scratch, without using any pre-trained models in contrast to most existing methods usually fine-tuned from the state-of-the-art pre-trained models, e.g. VGG-16, ResNet, etc. The experiments are conducted on four challenging scene labeling

datasets, i.e. SiftFlow, CamVid, Stanford background and SUN datasets, and compared against various state-of-the-art scene labeling methods.

References

Brostow, Gabriel J, Shotton, Jamie, Fauqueur, Julien, and Cipolla, Roberto. Segmentation and recognition using structure from motion point clouds. In *ECCV*, pp. 44–57, 2008.

Brostow, Gabriel J., Fauqueur, Julien, and Cipolla, Roberto. Semantic object classes in video: A high-definition ground truth database. *Pattern Recognition Letters*, 30(2):88–97, 2009.

Byeon, Wonmin, Breuel, Thomas M, Raue, Federico, and Liwicki, Marcus. Scene labeling with lstm recurrent neural networks. In *CVPR*, pp. 3547–3555, 2015.

Donahue, Jeff, Hendricks, Lisa Anne, Guadarrama, Sergio, Rohrbach, Marcus, Venugopalan, Subhashini, Saenko, Kate, and Darrell, Trevor. Long-term recurrent convolutional networks for visual recognition and description. In *CVPR*, 2015.

Everingham, M., Eslami, S. M. A., Van Gool, L., Williams, C. K. I., Winn, J., and Zisserman, A. The pascal visual object classes challenge: A retrospective. *ICCV*, 111(1): 98–136, 2015.

Fan, Heng, Mei, Xue, Prokhorov, Danil, and Ling, Haibin. Multi-level contextual rnns with attention model for scene labeling. *arXiv preprint arXiv:1607.02537*, 2016.

Farabet, Clement, Couprie, Camille, Najman, Laurent, and LeCun, Yann. Learning hierarchical features for scene labeling. *TPAMI*, 35(8):1915–1929, 2013.

Gould, Stephen, Fulton, Richard, and Koller, Daphne. Decomposing a scene into geometric and semantically consistent regions. In *ICCV*, pp. 1–8, 2009.

Graves, Alex. Offline arabic handwriting recognition with multidimensional recurrent neural networks. In *Guide to OCR for Arabic Scripts*, pp. 297–313. 2012.

He, Kaiming, Zhang, Xiangyu, Ren, Shaoqing, and Sun, Jian. Deep residual learning for image recognition. In *CVPR*, 2016a.

He, Kaiming, Zhang, Xiangyu, Ren, Shaoqing, and Sun, Jian. Identity mappings in deep residual networks. In *ECCV*, 2016b.

Liang, Ming, Hu, Xiaolin, and Zhang, Bo. Convolutional neural networks with intra-layer recurrent connections for scene labeling. In *NIPS*, pp. 937–945, 2015.

Lin, T. Y., Maire, M., Belongie, S., Hays, J., Perona, P., D. Ramanan and, P. Dollar, and Zitnick, C. L. Microsoft coco: Common objects in context. In *ECCV*, 2014.

Liu, Ce, Yuen, Jenny, and Torralba, Antonio. Nonparametric scene parsing: Label transfer via dense scene alignment. In *CVPR*, pp. 1972–1979, 2009.

Liu, Ce, Yuen, Jenny, and Torralba, Antonio. *Nonparametric Scene Parsing via Label Transfer*, pp. 207–236. Springer International Publishing, 2016.

Long, Jonathan, Shelhamer, Evan, and Darrell, Trevor. Fully convolutional networks for semantic segmentation. In *CVPR*, pp. 3431–3440, 2015.

Mnih, Volodymyr, Heess, Nicolas, Graves, Alex, et al. Recurrent models of visual attention. In *NIPS*, pp. 2204–2212, 2014.

Najafi, Mohammad, Taghavi Namin, Sarah, Salzmann, Mathieu, and Petersson, Lars. Sample and filter: Nonparametric scene parsing via efficient filtering. In *CVPR*, June 2016.

Pinheiro, Pedro HO and Collobert, Ronan. Recurrent convolutional neural networks for scene labeling. In *ICML*, pp. 82–90, 2014.

Rota Bulo, Samuel and Kontschieder, Peter. Neural decision forests for semantic image labelling. In *CVPR*, pp. 81–88, 2014.

Roy, Anirban and Todorovic, Sinisa. Scene labeling using beam search under mutex constraints. In *CVPR*, pp. 1178–1185, 2014.

Russakovsky, O., Deng, J., Su, H., Krause, J., Satheesh, S., Ma, S., Huang, Z., Karpathy, A., Khosla, A., Bernstein, M., and et al. Imagenet: large scale visual recognition challenge, 2014.

Sharma, Abhishek, Tuzel, Oncel, and Liu, Ming-Yu. Recursive context propagation network for semantic scene labeling. In *NIPS*, pp. 2447–2455, 2014.

Shotton, Jamie, Winn, John, Rother, Carsten, and Criminisi, Antonio. Textonboost: Joint appearance, shape and context modeling for multi-class object recognition and segmentation. In *ECCV*, pp. 1–15, 2006.

Shuai, Bing, Wang, Gang, Zuo, Zhen, Wang, Bing, and Zhao, Lifan. Integrating parametric and non-parametric models for scene labeling. In *CVPR*, pp. 4249–4258, 2015.

Shuai, Bing, Zuo, Zhen, Wang, Gang, and Wang, Bing. Dag-recurrent neural networks for scene labeling. In *CVPR*, 2016.

Souly, Nasim and Shah, Mubarak. Scene labeling using sparse precision matrix. In *CVPR*, June 2016.

Tighe, Joseph and Lazebnik, Svetlana. Superparsing: Scalable nonparametriv image parsing with superpixels. In *ECCV*, pp. 352–365, 2010.

Tighe, Joseph and Lazebnik, Svetlana. Finding things: Image parsing with regions and per-exemplar detectors. In *CVPR*, pp. 3001–3008, 2013.

Visin, Francesco, Kastner, Kyle, Courville, Aaron C., Bengio, Yoshua, Matteucci, Matteo, and Cho, KyungHyun. Reseg: A recurrent neural network for object segmentation. *CoRR*, abs/1511.07053, 2015.

Xiao, Jianxiong, Hays, James, Ehinger, Krista A, Oliva, Aude, and Torralba, Antonio. Sun database: Large-scale scene recognition from abbey to zoo. In *Computer vision and pattern recognition (CVPR), 2010 IEEE conference on*, pp. 3485–3492. IEEE, 2010.

Yang, Jimei, Price, Brian, Cohen, Scott, and Yang, Ming-Hsuan. Context driven scene parsing with attention to rare classes. In *CVPR*, pp. 3294–3301, 2014.

Zhang, Yimeng and Chen, Tsuhan. Efficient inference for fully-connected crfs with stationarity. In *CVPR*, pp. 582–589, 2012.

Zheng, Shuai, Jayasumana, Sadeep, Romera-Paredes, Bernardino, Vineet, Vibhav, Su, Zhizhong, Du, Dalong, Huang, Chang, and Torr, Philip HS. Conditional random fields as recurrent neural networks. In *CVPR*, pp. 1529–1537, 2015.

Zuo, Zhen, Shuai, Bing, Wang, Gang, Liu, Xiao, Wang, Xingxing, Wang, Bing, and Chen, Yushi. Convolutional recurrent neural networks: Learning spatial dependencies for image representation. In *CVPRW*, pp. 18–26, 2015.